Crystal and Magnetic Structures of 2H $BaMnO_3$

E. J. Cussen and P. D. Battle*

Inorganic Chemistry Laboratory, University of Oxford, South Parks Road, Oxford, United Kingdom OX1 3QR

Received September 17, 1999. Revised Manuscript Received December 23, 1999

The crystal structure of the 2H perovskite $BaMnO_3$ has been refined from neutron powder diffraction data collected at room temperature and 80 and 1.7 K. The structure consists of chains of face-sharing MnO_6 octahedra, separated by Ba^{2+} cations. At room temperature, $a = 5.6991(2)$, $c = 4.8148(2)$ Å, space group $P6_3/mmc$. At 80 K, $a = 9.8467(1)$, $c = 4.8075(1)$ Å, space group $P6_3cm$. The structural phase transition introduces a displacement of neighboring chains and reduces the coordination number of Ba^{2+}. Long-range antiferromagnetic ordering is apparent below $T_N = 59(2)$ K, with a magnetic moment of 1.31(5) μ_B per Mn^{4+} cation at 1.7 K. Neighboring spins within each chain are antiferromagnetically coupled and lie in a plane perpendicular to [001]. The spin directions associated with the chains at ($^1/_3$, $^2/_3$, z) and ($^2/_3$, $^1/_3$, z) are rotated by ±120° with respect to that of the chain at (0, 0, z).

Introduction

Recently, there has been considerable interest[1−7] in the magnetic properties of a group of materials which are structurally related to Sr_4PtO_6.[8] In that compound, alternating SrO_6 and PtO_6 polyhedra (trigonal prisms and octahedra, respectively) share triangular faces to form chains parallel to the z axis of a rhombohedral unit cell; the chains are separated by the remaining Sr cations. The current research activity was born of the realization that this structure is related to that (Figure 1) of the 2H perovskite compounds, for example $BaNiO_3$,[9] which contain chains of face-sharing octahedra parallel to z. The 2H perovskite ABO_3 can be considered to contain hexagonal close-packed (hcp) layers of stoichiometry A_3O_9, with the B cations occupying the resulting face-sharing, six-coordinate interlayer sites. The Sr_4PtO_6 structure type can be derived from this by removing (in an ordered manner) $^1/_3$ of the oxygen atoms from each layer to give it the stoichiometry A_3O_6 (Figure 2). The voids thus created can be filled with a cation, A′, and hence a layer of stoichiometry $A_3A'O_6$ is formed; the disposition of oxide ions in the hcp layers above and below the modified layer results in trigonal prismatic coordination of A′. This trigonal prismatic site within the layer nominally replaces two interlayer octahedral sites, and so it is the larger of the two types of six-coordinate site, although in practice the size difference is reduced by buckling of the layers. The Sr_4PtO_6 structure (A = A′ = Sr) results if every layer in the structure has stoichiometry $A_3A'O_6$. However, if layers of composition A_3O_9 are inserted into the hcp stacking sequence, it is possible to generate a large number of structures with different ratios of octahedral to trigonal prismatic sites in the chain. Darriet and Subramanian[10] have described a labeling scheme in which the structure can be described by the number, n, of consecutive $A_3A'O_6$ layers on either side of a single A_3O_9 layer. In this description, the Sr_4PtO_6 structure corresponds to $n = \infty$, and the 2H perovskite is the $n = 0$ end member. Much of the published work on these materials has been on Ni- or Co-containing compounds,[11−13] presumably as a result of $BaNiO_3$[9] and $BaCoO_{3-\delta}$[14,15] both being known to adopt the 2H structure. Materials based on the only other reported 2H oxide, $BaMnO_3$, had received little attention until we described the $n = 1$ phases $Ba_6Mn_4ZnO_{15}$ and $Ba_6Mn_4CuO_{15}$.[16] Interest in the magnetic properties of this structural family grew because the presence of polyhedral chains was expected to lead to unusual, one-dimensional (1D) magnetic behavior[17] which might be controlled chemically by varying the ratio of octahedra to prisms in the [001] chains. However, the data published to date[1,3,6] suggest that the interchain magnetic interactions are not negligible and that these materials should be treated as 3D magnets.

(1) Aasland, S.; Fjellvåg, H.; Hauback, B. *Solid State Comm.* **1997**, *101*, 187.
(2) Claridge, J. B.; Layland, R. C.; Henley, W. H.; Loye, H. C. z. *Chem. Mater.* **1999**, *11*, 1376.
(3) Darriet, J.; Grasset, F.; Battle, P. D. *Mater. Res. Bull.* **1997**, *32*, 139.
(4) Battle, P. D.; Blake, G. R.; Burley, J. C.; Cussen, E. J.; Sloan, J.; Vente, J. F.; Darriet, J.; Weill, F. *MRS Symp. Proc.* **1999**, *547*, 45.
(5) Kageyama, H.; Yoshimura, K.; Kosuge, K. *J. Solid State Chem.* **1998**, *140*, 14.
(6) Kawasaki, S.; Takano, M.; Inami, T. *J. Solid State Chem.* **1999**, *145*, 302.
(7) Lee, K. S.; Koo, H. J.; Whangbo, M. H. *Inorg. Chem.* **1999**, *38*, 2199.
(8) Randall, J. R.; Katz, L. *Acta Crystallogr.* **1959**, *12*, 519.
(9) Lander, J. J. *Acta Crystallogr.* **1951**, *4*, 148.
(10) Darriet, J.; Subramanian, M. A. *J. Mater. Chem.* **1995**, *5*, 543.
(11) Campa, J. A.; Gutiérrez-Puebla, E.; Monge, M. A.; Rasines, I.; Ruíz-Valero, C. *J. Solid State Chem.* **1994**, *108*, 230.
(12) Boulahya, K.; Parras, M.; González-Calbet, J. M. *J. Solid State Chem.* **1999**, *142*, 419.
(13) Boulahya, K.; Parras, M.; González-Calbet, J. M. *J. Solid State Chem.* **1999**, *145*, 116.
(14) Felser, C.; Yamaura, K.; Cava, R. J. *J. Solid State Chem.* **1999**, *146*, 411.
(15) Gushee, B. E.; Katz, L.; Ward, R. *J. Am. Chem. Soc.* **1957**, *79*, 5601.
(16) Cussen, E. J.; Vente, J. F.; Battle, P. D. *J. Am. Chem. Soc.* **1999**, *121*, 3958.
(17) Nguyen, T. N.; Lee, P. A.; zur-Loye, H.-C. *Science* **1996**, *271*, 489.

10.1021/cm991144j CCC: $19.00
Published on Web 02/29/2000

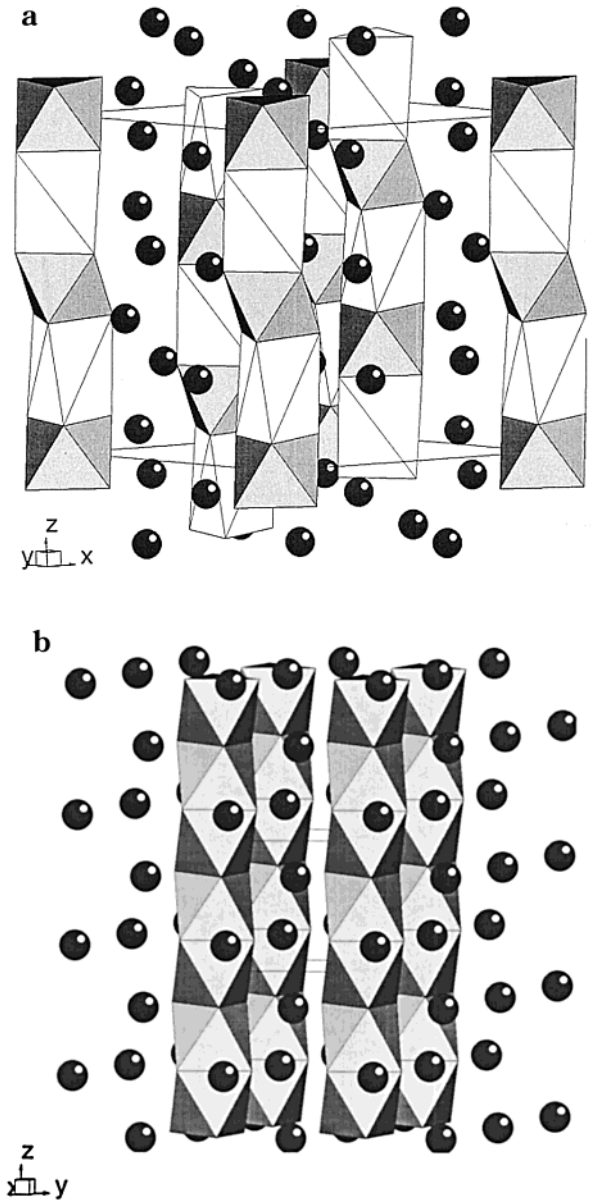

Figure 1. Crystal structure of (a) Sr_4PtO_6 and (b) 2H $BaNiO_3$. Filled circles represent alkaline earth cations, SrO_6 trigonal prisms are unshaded, and PtO_6 and NiO_6 octahedra are shaded.

This is exemplified by the high Néel temperature (90 K) of Ca_3NaRuO_6. During the course of our investigation into $Ba_6Mn_4ZnO_{15}$ and $Ba_6Mn_4CuO_{15}$, it became clear that the magnetic properties of $n = 0$ end-member $BaMnO_3$ were not well defined, and we have therefore undertaken a study of that compound in order to provide a reference point in the discussion of phases having $n > 0$. More specifically, we have determined T_N for $BaMnO_3$ and produced an improved model for the antiferromagnetic structure. We have also detected a lowering of the structural symmetry on cooling below room temperature.

Experimental Section

A polycrystalline sample of ca. 6 g of $BaMnO_3$ was prepared by standard solid-state techniques. $BaCO_3$ and MnO_2 were intimately mixed in the appropriate stoichiometric ratio, and the resulting powder was heated at 800 °C for 24 h in order to decompose the carbonate. The powder was then pressed into

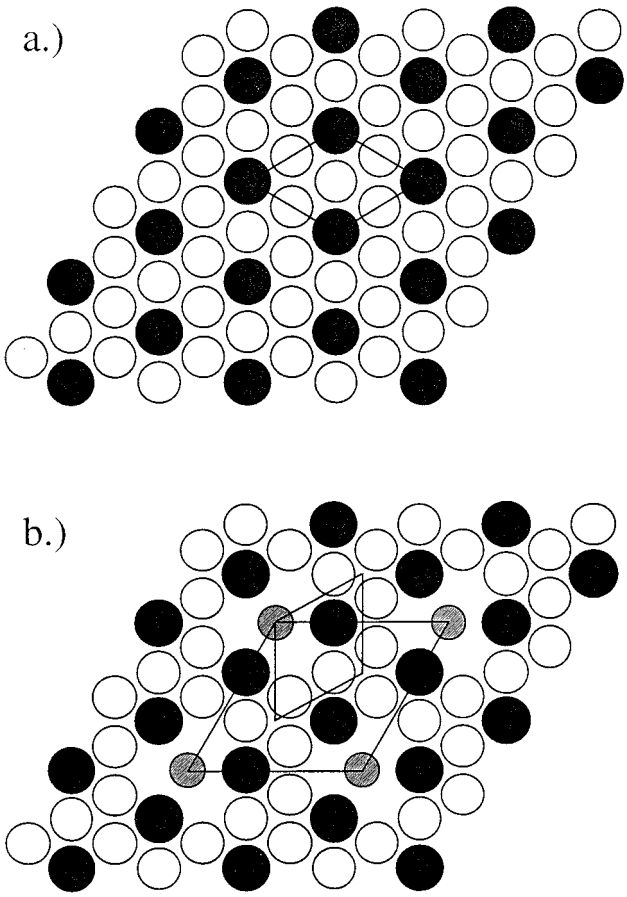

Figure 2. View along z of (a) A_3O_9 and (b) A_3O_6 layer with trigonal prismatic sites (A′) marked by lightly shaded circles. 2D (xy) unit cells are marked for both layer types, with $a' = \sqrt{3}a$.

five pellets of 12 mm diameter and heated at 900 °C for 1 day. Finally, the pelleted reactants were heated at 1000 °C for a total of 23 days, with regular regrinding and repelleting. All stages of the synthesis were carried out in air. The progress of the reaction was followed by X-ray diffraction, and it was judged to be complete when all of the peaks in the diffraction pattern could be indexed in the unit cell previously reported for $BaMnO_3$.[18] The oxygen content of the product was maximized by cooling to room temperature at a rate of 18 °C h^{-1} after the final heat treatment at 1000 °C. X-ray diffraction data were collected from this sample in the angular range $10 \leq 2\theta/° \leq 100$, $\Delta 2\theta = 0.02°$, using a Siemens D5000 diffractometer operating with Cu $K\alpha_1$ radiation in Bragg−Brentano geometry. High-resolution neutron diffraction data were collected at $\lambda = 1.5941$ Å over the angular range $10 \leq 2\theta/° \leq 148$, $\Delta 2\theta = 0.05°$, on the diffractometer D2b at the Institut Laue-Langevin (ILL), Grenoble. The sample was contained in a vanadium can of internal diameter 8 mm, and the temperature was regulated using an ILL orange cryostat; data were collected at room temperature and 80 and 1.7 K. The powder diffraction data were analyzed by profile analysis[19] as implemented in the GSAS suite of programs.[20] The background was described by a Chebyshev polynomial and the peak shape by a pseudo-Voigt function. No absorption correction was applied.

Additional neutron diffraction data were collected at $\lambda = 2.522$ Å using the instrument D1b at the ILL. This instrument utilizes a bank of 400 detectors which cover the angular range

(18) Chamberland, B. L.; Sleight, A. W.; Weiher, J. F. *J. Solid State Chem.* **1970**, *1*, 506.
(19) Rietveld, H. M. *J. Appl. Crystallogr.* **1969**, *2*, 65.
(20) Larson, A. C.; von-Dreele, R. B. *General Structure Analysis System (GSAS)*, Report LAUR 86-748; Los Alamos National Laboratories, 1990.

$10 \leq 2\theta/° \leq 90$. The counter bank remains stationary during the course of the experiment and enables rapid collection of a low-resolution diffraction pattern. This configuration was used to study the evolution of the magnetic structure of $BaMnO_3$ with temperature. The temperature was again controlled by an ILL orange cryostat and was programmed to increase linearly from 1.7 to 81.4 K over the course of 6 h. The data were summed, and the counters were reset to zero every 720 s, thus giving a temperature resolution of 2.66 K.

Magnetic measurements were made using an Quantum Design SQUID magnetometer. The susceptibility was determined in an applied field of 1 kG after cooling of the sample in both zero applied field (ZFC) and the measuring field (FC).

Results

The X-ray diffraction pattern collected from the product at room temperature could be indexed in the space group $P6_3/mmc$ using a structural model consisting of [001] chains of face-linked MnO_6 octahedra separated by chains of Ba^{2+} cations, as has been described previously for $BaMnO_3$.[18,21,22] Rietveld refinement of this model gave a satisfactory fit to the overall profile. However, while the fwhm of the $hk0$ reflections approached the instrumental resolution, the hkl, $l \neq 0$ reflections showed a degree of broadening, and the refinement therefore required the use of the anisotropic peak broadening coefficient available in GSAS. This is consistent with the highly anisotropic nature of the crystal structure; similar effects have been observed previously in related compounds.[23] In addition to the reflections associated with the 2H $BaMnO_3$ structure, the neutron diffraction data collected at room temperature using the diffractometer D2b contained peaks of low intensity which could be attributed to the presence of a small quantity (1.6(8)%) of the 15R $BaMnO_{3-\delta}$ phase reported by Negas and Roth.[22] This impurity was masked in the X-ray data by the background noise. A detailed structural analysis was carried out by analyzing the X-ray and neutron data sets simultaneously, with both 2H and 15R phases present. The use of X-ray data in the refinement increased the estimated standard deviations (esd's) of the lattice parameters, but they remained acceptable; in addition, the Durbin−Watson d-statistic (DW-d)[24] indicated that the simultaneous use of both data sets reduced the serial correlations in the refinement, thus suggesting that the calculated esd's are likely to be closer to the true values. More importantly, the well-defined wavelength of the Cu $K\alpha_1$ radiation allowed refinement of the neutron wavelength, thus reducing the systematic errors in the refined lattice parameters which can be caused by slight misalignment of the neutron monochromator. The resulting increase in accuracy, at the expense of a small loss in precision, justifies the use of a simultaneous refinement. Trial refinements of the fractional occupancy of the oxygen site in the 2H phase resulted in a value of 1.08(5), indicating that, within the precision of the data, the site is fully occupied, as would be expected from the synthetic conditions. This conclusion is also consistent with the color of the sample, which was dark green rather than black. The occupancy was subsequently held constant with a value of unity. Anisotropic temperature factors were refined freely within the constraints imposed by the atomic site symmetry. The refinement thus utilized a total of 37 variables to describe the 2H phase: 2 scale factors, 1 phase fraction, 2 zero points, 1 neutron wavelength, 2 lattice parameters, 7 anisotropic temperature factor parameters, 1 atomic position, 6 neutron profile parameters, 3 X-ray profile parameters, 6 neutron background parameters, and 6 X-ray background parameters. The structural parameters of the minor 15R component were held constant. The resulting atomic positions, thermal parameters, and interatomic distances for the 2H phase are given in Tables 1, 2 and 3, respectively. The fitted X-ray and neutron diffraction patterns are presented in Figure 3. The residual fit parameters for the neutron and X-ray data are $R_{wp} = 6.28$, $R_p = 4.68$, $R_I = 2.36$, and DW-d = 0.533 and $R_{wp} = 8.74$, $R_p = 6.83$, and DW-d = 1.681,[24] respectively, with a total $\chi^2_{red} = 2.512$ for 37 variables. The low values of the parameter DW-d show that, as is usual in Rietveld refinements, the errors in the refined parameters are underestimated as a consequence of serial correlations in adjacent residuals. In common with Christensen and Ollivier[25] but contrary to the earlier study by Hardy,[21] we found no evidence to suggest that the room temperature structure is better described in the noncentrosymmetric space group $P6_3mc$. Interestingly, the unit cell parameters listed in Table 1 are in reasonable agreement with the majority of previous determinations[18,22,25] but significantly larger than those determined by Hardy.

Initial attempts to analyze the neutron diffraction data collected at 80 K used the structural model described above, but it became evident that the diffraction pattern contained a number of weak peaks which had not been observed at room temperature. These peaks were distributed over the full angular range, indicating that not all (if any) of them could be due to the presence of long-range magnetic ordering. The full

Table 1. Structural Parameters of $BaMnO_3$ at Room Temperature[a]

atom	site	x	y	z
Ba	2d	$^1/_3$	$^2/_3$	$^3/_4$
Mn	2a	0	0	0
O	6h	0.14950(5)	0.2990(1)	$^1/_4$

[a] Space group $P6_3/mmc$: $a = 5.6991(2)$ Å, $c = 4.8148(2)$ Å, $V = 135.43(1)$ Å^3.

Table 2. Temperature Factors (Å^2) of $BaMnO_3$ at Room Temperature[a]

atom	U_{11}	U_{22}	U_{33}	U_{12}
Ba	0.0070(4)	0.0070(4)	0.0216(8)	0.0035(2)
Mn	0.0061(4)	0.0061(4)	0.0078(8)	0.0030(2)
O	0.0092(2)	0.0076(3)	0.0113(3)	0.0038(2)

[a] $U_{13} = U_{23} = 0$ for all atoms.

Table 3. Bond Lengths (Å) and Angles (deg) in $BaMnO_3$ at Room Temperature

Ba−O	2.8546(1) × 6	Mn−O	1.9044(4) × 6
Ba−O	3.0147(3) × 6	Mn−Mn	2.4074(1)
shortest O−O	2.5561(9)		
O−Mn−O	84.30(2)	Mn−O−Mn	78.41(2)

(21) Hardy, A. *Acta Crystallogr.* **1962**, *15*, 179.
(22) Negas, T.; Roth, R. S. *J. Solid State Chem.* **1971**, *3*, 323.
(23) Battle, P. D.; Burley, J. C.; Cussen, E. J.; Darriet, J.; Weill, F. *J. Mater. Chem.* **1999**, *9*, 479.
(24) Hill, R. J.; Flack, H. D. *J. Appl. Crystallogr.* **1987**, *20*, 356.
(25) Christensen, A. N.; Ollivier, G. *J. Solid State Chem.* **1972**, *4*, 131.

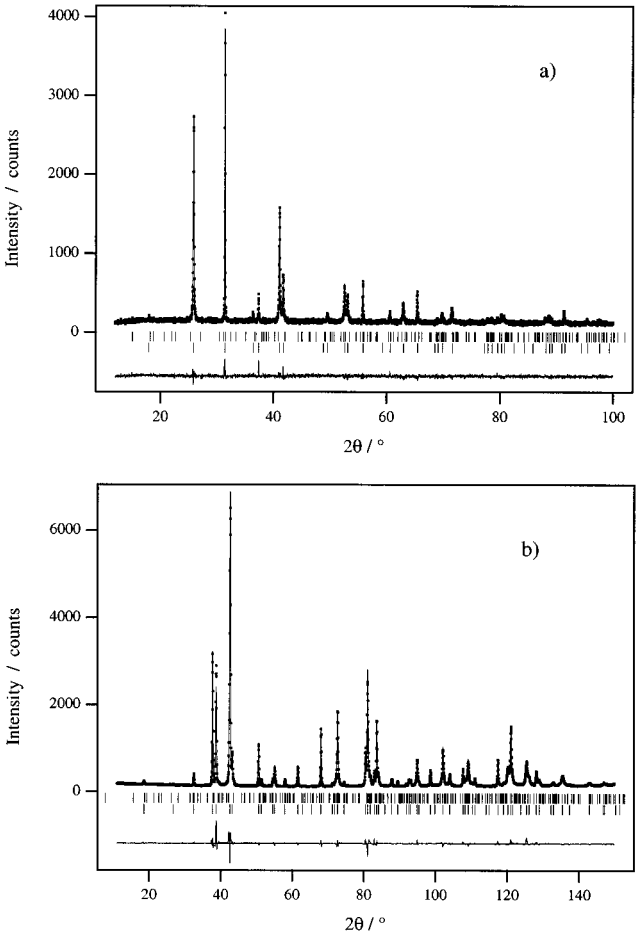

Figure 3. Observed, calculated, and difference (a) X-ray and (b) neutron powder diffraction patterns for $BaMnO_3$ at room temperature. Tick marks indicate the reflection positions for both the impurity (upper) and principal (lower) phases.

set of peaks was eventually indexed in a hexagonal unit cell with a volume three times greater than that observed at room temperature, the expansion taking place in the *xy* plane. Specifically, if the unit cell parameters at room temperature are a_0 and c_0, those at 80 K are $a' \sim \sqrt{3}a_0$ and $c' \sim c_0$; in vector terms, $\mathbf{a'} = \mathbf{a_0} - \mathbf{b_0}$, $\mathbf{b'} = \mathbf{a_0} + 2\mathbf{b_0}$, $\mathbf{c'} = \mathbf{c_0}$. The systematic absences in the diffraction pattern were consistent with the retention of symmetry in space group $P6_3/mcm$, but it was necessary to adopt the noncentrosymmetric subgroup $P6_3cm$ in order to achieve a satisfactory refinement. In the absence of a center of symmetry, an atom position had to be fixed in order to define an origin, and the Mn cation occupying the 2*a* site, position 0, 0, *z*, was therefore held at $z = 0$. The increased number of variable atomic coordinates in the enlarged unit cell reduced the stability and precision of the refinement, and it was not possible to allow for any anisotropic character in the thermal motion of the atoms. The atomic coordinates and isotropic temperature factors resulting from the refinement of this model are given in Tables 4 and 5, respectively. The residual fit parameters for the fit shown in Figure 4 are $R_{wp} = 6.12$, $R_p = 4.76$, $R_I = 3.31$, DW-$d = 0.768$, and $\chi^2_{red} = 2.532$ for 29 variables. No magnetic scattering was included in the data analysis. An account of the distorted 2H structure of $RbVBr_3$ has discussed ambiguity in the choice of space group between $P6_3cm$ and $P\bar{3}c1$, a centrosymmetric

Table 4. Structural Parameters of $BaMnO_3$ at 80 K[a]

atom	site	*x*	*y*	*z*	U_{iso}
Ba(1)	6c	0.332(2)	0.332(2)	0.238(5)	0.0047(5)
Mn(1)	2a	0	0	0	−0.002(8)
Mn(2)	4b	$^2/_3$	$^1/_3$	0.963(3)	0.007(5)
O(1)	6c	0	0.150(2)	0.250(5)	0.005(4)
O(2)	12d	0.667(1)	0.484(1)	0.212(5)	0.006(2)

[a] Space group $P6_3cm$: $a = 9.8467(1)$ Å, $c = 4.8075(1)$ Å, $V = 403.68(1)$. The 15R $BaMnO_3$ impurity concentration was held at its room temperature value (1.6(8)%)

Table 5. Bond Lengths (Å) and Angles (°) in $BaMnO_3$ at 80 K

Ba−O(1)	2.84(2) × 2	Mn(1)−O(1)	1.90(2) × 3
Ba−O(2)	2.84(1) × 2	Mn(1)−O(1)	1.91(2) × 3
Ba−O(2)	2.86(2) × 2	Mn(2)−O(2)	1.90(1)
Ba−O(2)	2.91(1) × 2	Mn(2)−O(2)	1.90(2)
Ba−O(1)	2.95(2)		
Ba−O(1)	3.05(2)	O(2)−O(2)	2.55(2)
Ba−O(2)	3.109(9) × 2		
O(1)−Mn(1)−O(1)	84.4(10)	O(2)−Mn(2)−O(2)	84.2(7)
O(1)−Mn(1)−O(1)	84.5(11)	O(2)−Mn(2)−O(2)	84.4(8)
O(1)−Mn(1)−O(1)	179.929(1)	O(2)−Mn(2)−O(2)	179.508(7)
Mn(1)−O(1)-Mn(1)	78.2(7)	Mn(2)−O(2)-Mn(2)	78.4(4)

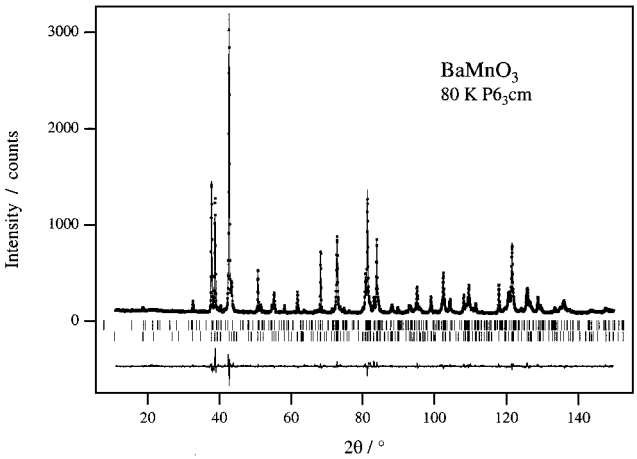

Figure 4. Observed, calculated, and difference neutron powder diffraction patterns for $BaMnO_3$ at 80 K. Tick marks indicate the reflection positions for both the impurity (upper) and principal (lower) phases.

subgroup of $P6_3/mcm$.[26] A trial refinement in $P\bar{3}c1$ revealed a similar ambiguity in the case of $BaMnO_3$, and we too are therefore unable to rule out the possibility that the low-temperature phase is trigonal rather than hexagonal. Careful analysis of Friedel pairs collected from a single crystal would be needed to resolve this point. Our choice of space group $P6_3cm$ to describe the low-temperature phase is thus somewhat arbitrary. However, the principal result of our work, that is, the determination of the magnetic structure of $BaMnO_3$, does not hinge on this choice.

The high-angle region of the diffraction pattern collected at 1.7 K resembled that recorded at 80 K, although the intensities of the superlattice reflections were somewhat increased. In addition, the pattern contained three low-angle peaks which were not observed at 80 K. These peaks, which we shall show below to be magnetic in origin, were observed, with similar relative intensities, by Christensen and Ollivier[25] in an

(26) Hauser, A.; Falk, U.; Fischer, P.; Güdel, H. U. *J. Solid State Chem.* **1985**, *56*, 343.

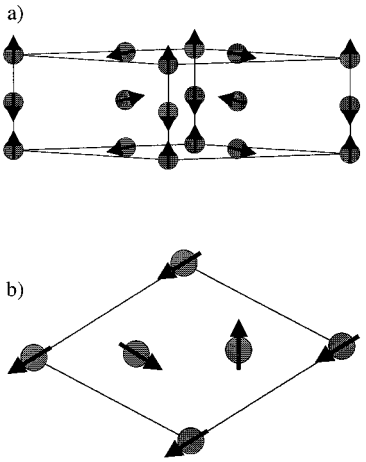

Figure 5. Magnetic structure of $BaMnO_3$: (a) viewed perpendicular to [001] with arrows indicative of relative (not absolute) spin directions and (b) viewed along [001] with arrows representing the actual spin directions of Mn cations with $z \sim 0$.

Table 6. Structural Parameters of $BaMnO_3$ at 1.7 K[a]

atom	site	x	y	z	U_{iso} (Å^2)
Ba(1)	6c	0.339(1)	0.339(1)	0.230(5)	0.0028(7)
Mn(1)	2a	0	0	0	0.006(4)
Mn(2)	4b	$^2/_3$	$^1/_3$	0.952(3)	0.000(2)
O(1)	6c	0	0.1492(5)	0.248(6)	−0.003(2)
O(2)	12d	0.6644(8)	0.4824(5)	0.200(6)	0.009(1)

[a] Space group $P6_3cm$ no. 185; $a = 9.8444(1)$ Å, $c = 4.8082(1)$ Å, $V = 403.54(1)$ Å^3. The 15R $BaMnO_3$ impurity concentration remained at its room temperature value (1.6(8)%).

earlier study and indexed using a $\sqrt{3}a_0 \times \sqrt{3}a_0 \times c_0$ unit cell. However, the greatly increased precision of our measurement allowed us to deduce that the model used to fit the data in the previous study is an incorrect description of the magnetic structure at this temperature. Our data were better fitted using a noncollinear arrangement of the moments which has commonly been observed in 2H halides.[26−28] The magnetic model employed here involves antiferromagnetic ordering along each chain with the orientation of the moments in each of the three chains differing by 120°. The best refinement was achieved when the moments were constrained to lie in the (001) plane, as in $CsVI_3$.[29] This arrangement is shown schematically in Figure 5. The final refinement was carried out with the orientation of the moments fixed in this ideal arrangement and with the moment on each Mn^{4+} cation constrained to take the same value. The moment refined to a value of 1.31(5) μ_B per Mn^{4+}. The crystal structure was refined simultaneously with the magnetic structure, taking the coordinates in Table 4 as a starting point. The final values calculated for the atomic parameters, isotropic temperature factors, and bond lengths at 1.7 K are given in Tables 6 and 7. The residual fit parameters for the data shown in Figure 6 are $R_{wp} = 6.00$, $R_p = 4.567$, $R_I = 3.96$, $R_M = 8.02$, DW-d = 0.846, and $\chi^2_{red} = 2.092$ for the 30 variables utilized in fitting the data collected at 80 K plus an additional parameter describing the magnitude of the ordered magnetic moment. Refinements were also attempted in which the constraint on the magnitude of the moments was partially removed; the magnetic moments of the crystallographically distinct Mn cations were allowed to take differing values, but the canting angle between moments in neighboring chains remained fixed at 120°. These refinements failed to converge.

Table 7. Bond Lengths (Å) and Angles (deg) of $BaMnO_3$ at 1.7 K

Ba(1)−O(1)	2.783(8) × 2	Mn(1)−O(1)	1.89(2) × 3
Ba(1)−O(1)	2.866(7) × 2	Mn(1)−O(1)	1.90(2) × 3
Ba(1)−O(1)	2.870(7) × 2	Mn(2)−O(2)	1.90(1) × 3
Ba(1)−O(2)	2.900(9) × 2	Mn(2)−O(2)	1.91(1) × 3
Ba(1)−O(2)	2.978(9) × 1	Mn(1)−Mn(1)	2.40411(6)
Ba(1)−O(2)	3.107(8) × 2	Mn(2)−Mn(2)	2.40411(6)
Ba(1)−O(2)	3.12(1) × 1	O(1)−O(1)	2.545(9)
O(1)−Mn(1)-O(1)	84(1)	O(2)−Mn(2)-O(2)	84.1(7)
O(1)−Mn(1)-O(1)	85(1)	O(2)−Mn(2)-O(2)	84.9(7)
O(1)−Mn(1)-O(1)	95.8(2)	O(2)−Mn(2)-O(2)	94.8(3)
O(1)−Mn(1)-O(1)	179.615(9)	O(2)−Mn(2)-O(2)	178.7(6)
Mn(1)−O(1)-Mn(1)	78.6(2)	Mn(2)−O(2)-Mn(2)	78.2(1)

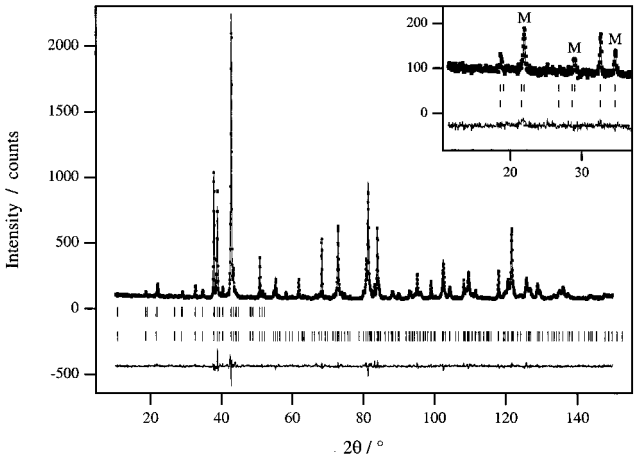

Figure 6. Observed, calculated, and difference neutron powder diffraction patterns for $BaMnO_3$ at 1.7 K. Upper and lower reflection markers correspond to magnetic and nuclear scattering, respectively. The fit to the principal magnetic peaks (M) is emphasized in the inset.

The data collected on D1b were analyzed in order to establish the temperature dependence of the long-range ordered magnetic moment. All of the data sets collected using this instrument contained a feature in the angular range $71.4 \leq 2\theta/° \leq 73.2$ which was not observed in the D2b data; this feature is also present in data collected from other samples on D1b. It is therefore believed to be instrumental in origin, and the data in this angular range were excluded from the analysis. The data collected on D1b contained only a small number of nuclear reflections, which showed considerable peak overlap due to the low resolution of the instrument. Our Rietveld refinements therefore utilized only a limited number of variables. The atomic coordinates were fixed at the values derived from the D2b experiment performed at 1.7 K, and only the lattice parameters, profile parameters, background parameters, scale factor, counter zero-point error, and magnetic moment were refined. This model could satisfactorily be refined against every data set to give weighted residual fit parameters $R_{wp} < 3.0\%$. The data collected at 34.4 K are shown in Figure 7 and provide an indication of the quality of fit typically obtained. The variation with temperature of the ordered magnetic moment extracted from these refinements is shown in Figure 8. The moment decreases in the

(27) Zandbergen, H. W.; Ijdo, D. J. W. *J. Solid State Chem.* **1981**, *38*, 199.
(28) Zandbergen, H. W. *J. Solid State Chem.* **1980**, *35*, 367.
(29) Zandbergen, H. W. *J. Solid State Chem.* **1981**, *37*, 308.

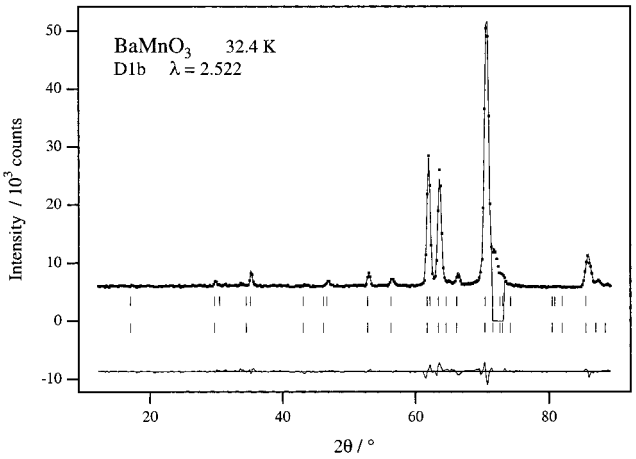

Figure 7. Observed, calculated, and difference neutron powder diffraction patterns for $BaMnO_3$ taken on D1b at 32.4 K.

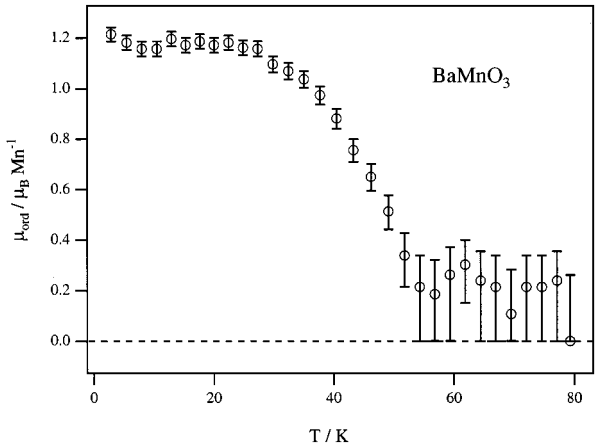

Figure 8. Temperature dependence of the Mn^{4+} ordered magnetic moment in $BaMnO_3$.

temperature range $2.8 < T < 59.4$ K from 1.21(6) μ_B to a value of ca. 0.2(2) μ_B and then does not decrease further in the measured temperature range. Inspection of the diffraction patterns collected at the higher temperature limit showed that the magnetic peaks which had been identified at 1.7 K were no longer evident. The small, nonzero values obtained from the refinements against data collected at temperatures greater than 59-(2) K are therefore due to the noise in the background. We deduce a value of 59(2) K for the Néel temperature of $BaMnO_3$.

The temperature dependence of the magnetic susceptibility of this sample measured in a field of 1000 G is shown in Figure 9. Curie-Weiss paramagnetic behavior is not observed in any region of the measured temperature range and below 215 K the field-cooled (FC) and zero-field-cooled (ZFC) data diverge. The onset of long-range antiferromagnetic ordering is usually associated with a maximum in the magnetic susceptibility, but these data show no evidence of such a transition.

Discussion

High-resolution neutron diffraction experiments have allowed us to confirm the room temperature structure of $BaMnO_3$ reported previously. The Mn−O bond lengths extracted from our room temperature data are similar

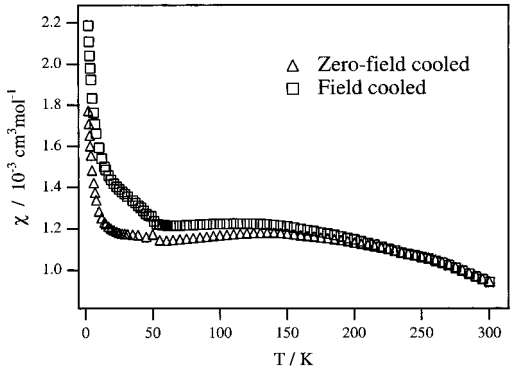

Figure 9. Temperature dependence of the molar magnetic susceptibility of $BaMnO_3$ measured after zero-field cooling and after cooling in the measuring field of 1 kG.

to the longer group of three distances found in 4H $SrMnO_3$,[30] and thus somewhat longer than the mean distance (1.889 Å) found in that compound. They are also longer than the mean Mn−O distance (1.897 Å) found in the $n = 3$ Ruddlesden−Popper phase $Ca_4Mn_3O_{10}$.[31] However, the value of these comparisons is limited by the precision of the bond lengths determined in the earlier studies (ca. ±0.006 Å). A more striking and less ambiguous observation is that the Mn−Mn distance across the shared octahedral face is remarkably short (2.4074(1) Å) in $BaMnO_3$; the corresponding distance in $SrMnO_3$ is 2.500(6) Å. The latter value is consistent with the Mn−Mn separations of 2.494(8) and 2.513(5) Å observed in the Mn_2O_9 dimers of 4H $Ba_{0.1}Sr_{0.9}MnO_{2.96}$[32] and 15R $SrMn_{0.9}Fe_{0.1}O_{2.979}$,[33] respectively. In both of these cases, the linking of the dimers to neighboring octahedra by vertex sharing, rather than face sharing, facilitates a displacement of the Mn cations within the dimers away from the center of the octahedral site, and hence away from the shared face, thus reducing the electrostatic repulsion between them. In the infinite chains of the 2H structure, no cooperative displacement can achieve this effect and the Mn^{4+} cations reside at the centers of the octahedra. The shortest O−O distance (2.5561(9) Å) found in $BaMnO_3$ is a result of the oxide ions moving to partially screen the electrostatic repulsion between the Mn^{4+} cations. However, this distance is longer than that found between the corresponding anions in 15R $SrMn_{0.9}Fe_{0.1}O_{2.979}$, presumably a consequence of the presence of the relatively large Ba^{2+} cations. The Mn cations could reduce their mutual repulsion by disordering in the *xy* plane, but there is no evidence for this in the thermal parameters.

$BaMnO_3$ undergoes a structural distortion on cooling from room temperature to 80 K; we have not established the actual transition temperature. The low-temperature phase can be described in two space groups, $P6_3cm$ and $P\bar{3}c1$, although we have chosen only to present our results in the former, which has the higher symmetry. The three MnO_6 chains contained in the unit cell are

(30) Battle, P. D.; Gibb, T. C.; Jones, C. W. *J. Solid State Chem.* **1988**, *74*, 60.
(31) Battle, P. D.; Green, M. A.; Lago, J.; Millburn, J. E.; Rosseinsky, M. J.; Vente, J. F. *Chem. Mater.* **1998**, *10*, 658.
(32) Jacobson, A. J.; Horrox, A. J. W. *Acta Crytallogr. B* **1976**, *32*, 1003.
(33) Cussen, E. J.; Sloan, J.; Vente, J. F.; Battle, P. D.; Gibb, T. C. *Inorg. Chem.* **1998**, *37*, 6071.

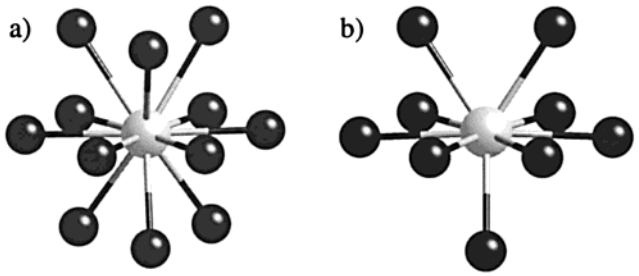

Figure 10. Coordination environment of Ba^{2+} within a radius of 3.05 Å at (a) room temperature and (b) 1.7 K.

not all crystallographically equivalent in either, with those along $^1/_3$, $^2/_3$, z and $^2/_3$, $^1/_3$, z being related to each other but distinct from that along 0, 0, z. The inability of the data to distinguish between the two space groups is a consequence of the regularity of the MnO_6 octahedra. A consideration of the structural parameters extracted from the data collected at 80 K shows that the phase transition is driven by a relative displacement of the octahedral chains and the consequent changes in the coordination environment of the Ba cations. On cooling from room temperature, three of the Ba−O bond lengths increase from 3.0147(3) to 3.06(2) and 3.07(2) Å, suggesting that the coordination of the Ba cations has been reduced from 12 at room temperature to 9 at 80 K. The six neighbors in the same BaO_3 plane as the cation are retained (Figure 10), but the distances to three of the anions in neighboring planes increase by ∼0.1 Å. However, as the bond lengths in Tables 3 and 5 show, within the precision of the refinements the Mn−O distances are largely invariant between room temperature and 80 K; the chains are displaced without distortion. The change in the coordination of Ba, as well as the absence of any change in that of Mn, is emphasized by the results of the analysis of the data collected at 1.7 K; the greater distortion at the lower temperature leads to an improvement in the precision of the derived bond lengths. The temperature dependence of the unit cell volume is interesting. On cooling the sample from room temperature to 80 K, a reduction in volume per formula unit of 0.647(3)% occurs, whereas the unit cell undergoes a further reduction in volume of only 0.032(8)% on cooling from 80 to 1.7 K. The large difference between these two values provides an indication of the magnitude of the volume change associated with the phase transition which occurs between room temperature and 80 K. This volume change is not isotropic. The c lattice parameter decreases by 0.151(3)% over this temperature range, whereas the a parameter is reduced by 0.262(4)%. This observation is reasonable when the origin of the distortion is considered. In $BaMnO_3$, the c parameter is a dependent on both the bond lengths and angles in the MnO_6 chains and the Ba coordination. However, as the chains are not directly linked but are separated by Ba cations, the a lattice parameter can change without any modification to the coordination geometry of the Mn cations. Changes in the Ba−O distances are therefore best accommodated by changes in the dimensions of the xy plane of the unit cell.

The canted antiferromagnetically ordered state observed at 1.7 K has not been observed previously in a 2H metal oxide. The neutron diffraction study of Christensen and Ollivier[25] observed magnetic Bragg peaks of similar intensity and d spacing but used a collinear antiferromagnetic model to fit the diffraction profile. Increases in instrument resolution and flux have allowed us to show this model to be incorrect. The antiferromagnetic coupling along each of the [001] polyhedral chains is to be expected in view of the $3d^3$ electron configuration of Mn^{4+} and the very short Mn−Mn distance in this direction. The canted arrangement of the moments in the xy plane, a consequence of the triangular lattice formed by the Mn cations, is more interesting. In the room temperature structure, space group $P6_3/mmc$, each Mn cation is equidistant, at 5.6991(2) Å, from 6 neighboring Mn cations in the same interstitial layer between the close-packed BaO_3 sheets. The magnetic interactions between these cations are antiferromagnetic, and it is therefore not possible for cations occupying this lattice to adopt a nonfrustrated, collinear, antiferromagnetically ordered phase, and a 120° spin structure would be expected to result. The lower symmetry of $BaMnO_3$ at 80 and 1.7 K formally removes this equivalence; the six superexchange pathways are no longer identical, and the strength of the interaction can therefore vary. However, the 120° model provides an excellent fit to the data, suggesting that in $BaMnO_3$ the variation in strength of the superexchange interactions as a consequence of the structural distortion is small. The reduction (∼60%) of the ordered component of the Mn^{4+} magnetic moment from the maximum value $gS = 3\,\mu_B$ is comparable to that seen in the isostructural, isoelectronic compound $CsVCl_3$ and is attributed[26,34,35] to the effects of covalency and the enhanced zero-point motion observed in these systems.[35] The fact that the effect is as strong in an oxide as that in the halides suggests that zero-point effects are more significant than covalency.

Variable-temperature neutron diffraction experiments have shown unequivocally that the Néel temperature of this material is 59(2) K, significantly greater than the upper limit of 2.4 K proposed previously.[25] The occurrence of 3D magnetic ordering at a temperature as high as this demonstrates that consideration of a 2H perovskite oxide as a purely 1D structure is invalid below room temperature (300 K ∼ $5T_N$). While the 2H structure is rare among oxides, the structurally related compounds referred to above which contain both trigonal prismatic and octahedral cation sites in the polyhedral chain have been the subject of considerable research, much of which has been driven by the belief that their electronic properties will show 1D behavior. It has been shown previously that such materials can show long-range magnetic order at temperatures up to $T_N = 120$ K in cases where half of the polyhedra in the chain are occupied by diamagnetic species.[3,4] The interchain interactions which lead to 3D magnetic ordering cannot, therefore, be considered negligible compared to the intrachain interactions in either the magnetically concentrated case of the $n = 0$ 2H perovskite structure or in the case of magnetically dilute, $n = \infty$ phases. This view has recently received support from extended Hückel calculations.[7]

(34) Hirakawa, K.; Yoshizawa, H.; Ubukoshi, K. *J. Phys. Soc. Jpn.* **1982**, *51*, 1119.
(35) Kadowaki, H.; Hirakawa, K.; Ubukoshi, K. *J. Phys. Soc. Jpn.* **1983**, *52*, 1799.

A previous study of the 2H solid-solution $BaCo_{1-x}Mn_xO_3$ reported that the magnetic susceptibility of $BaMnO_3$ obeys the Curie−Weiss law above 77 K, the lowest temperature measured.[36] That study also found that the data for the solid solution could be rationalized using a spin-only contribution to the paramagnetic susceptibility from Mn^{4+} and Co^{4+}, the latter undergoing a high- to low-spin transition at $x \sim 0.5$. The magnetic susceptibility of our sample does not agree with this observation. Paramagnetic Curie−Weiss behavior was not observed in any portion of the measured temperature range, but instead, the material showed a small susceptibility which was relatively insensitive to temperature. The value measured at 300 K is ∼15% of the value predicted by the Curie Law for a system of noninteracting Mn^{4+} cations. The magnetic properties of 2H halides have been more widely studied than oxides and so can be usefully employed to draw some qualitative comparisons with these data. Similar observations have been made in 2H halides AVX_3 (A = Rb, Cs; X = Cl, Br, I) containing V^{2+} which is isoelectronic with Mn^{4+}.[26] The low value of the susceptibility is due to the short intrachain superexchange pathways. In the present case, it is likely that neighboring spins within the individual chains are antiferromagnetically coupled at room temperature, and this is responsible for the low value of the observed susceptibility. There is evidence for spin pairing within the Mn_2O_9 dimers of $SrMnO_3$ at 300 K,[18,30] and we have observed a similar effect in $Ba_6Mn_4ZnO_{15}$ which contains an oxide chain composed of a mixture of octahedral and trigonal prismatic coordination sites in a 4:1 ratio.[16] The formation of a long-range antiferromagnetically ordered phase at 59 K is thus not a transition from a paramagnetic material but rather from a one-dimensionally antiferromagnetically ordered phase, and the formation of a three-dimensionally magnetically ordered material at T_N is therefore not signaled by a reduction in the magnetic susceptibility. The DC magnetic susceptibilities of 2H halides AVX_3 (A = Rb, Cs; X = Cl, Br, I) do not show any evidence of long-range magnetic order around the Néel temperatures, determined by neutron diffraction, which varied between 13.8 K, for $CsVCl_3$, and 34.8 K, for $CsVI_3$.[26] The ordering temperature is slightly higher in the present case presumably due to the shorter interatomic distances in the oxide. The low-temperature tail in the susceptibility data in Figure 9 might be due to the presence of the low concentration of a second phase which was detected by neutron diffraction. It is not clear whether the hysteresis between the field-cooled and zero-field-cooled data is a consequence of the impurity or an intrinsic property of the principal phase.

In conclusion, we have shown that the 2H perovskite $BaMnO_3$ undergoes a structural phase transition between room temperature and 80 K and that it adopts a noncollinear antiferromagnetic spin structure below 59(2) K.

Acknowledgment. We are grateful to EPSRC for financial support and to Thomas Hansen for experimental assistance at ILL, Grenoble.

CM991144J

(36) Taguchi, H.; Shimada, M.; Kanamaru, F.; Koizumi, M.; Takeda, Y. *J. Solid State Chem.* **1976**, *18*, 299.